

VU Research Portal

Simulation of the Impact of Environmental Disturbances on Forest Biomass in Taiwan

Chen, Yi Ying; Huang, Wei; Cheng, Chao Tzuen; Hong, Jing Shan; Yeh, Fang Li; Luysaert, Sebastiaan

published in

Journal of Geophysical Research: Biogeosciences
2022

DOI (link to publisher)

[10.1029/2021JG006519](https://doi.org/10.1029/2021JG006519)

document version

Publisher's PDF, also known as Version of record

document license

Article 25fa Dutch Copyright Act

[Link to publication in VU Research Portal](#)

citation for published version (APA)

Chen, Y. Y., Huang, W., Cheng, C. T., Hong, J. S., Yeh, F. L., & Luysaert, S. (2022). Simulation of the Impact of Environmental Disturbances on Forest Biomass in Taiwan. *Journal of Geophysical Research: Biogeosciences*, 127(3), 1-15. [e2021JG006519]. <https://doi.org/10.1029/2021JG006519>

General rights

Copyright and moral rights for the publications made accessible in the public portal are retained by the authors and/or other copyright owners and it is a condition of accessing publications that users recognise and abide by the legal requirements associated with these rights.

- Users may download and print one copy of any publication from the public portal for the purpose of private study or research.
- You may not further distribute the material or use it for any profit-making activity or commercial gain
- You may freely distribute the URL identifying the publication in the public portal ?

Take down policy

If you believe that this document breaches copyright please contact us providing details, and we will remove access to the work immediately and investigate your claim.

E-mail address:

vuresearchportal.ub@vu.nl

JGR Biogeosciences

RESEARCH ARTICLE

10.1029/2021JG006519

Key Points:

- Findings show a greater decrease in forest biomass due to tropical cyclones than to the effects of changes in LULC, CO₂ and climate
- Models which do not consider wind disturbance may greatly overestimate the forest biomass in regions prone to frequent tropical cyclones

Supporting Information:

Supporting Information may be found in the online version of this article.

Correspondence to:

Y.-Y. Chen,
yyingchen@gate.sinica.edu.tw

Citation:

Chen, Y.-Y., Huang, W., Cheng, C.-T., Hong, J.-S., Yeh, F.-L., & Luysaert, S. (2022). Simulation of the impact of environmental disturbances on forest biomass in Taiwan. *Journal of Geophysical Research: Biogeosciences*, 127, e2021JG006519. <https://doi.org/10.1029/2021JG006519>





Received 13 JUL 2021

Accepted 4 MAR 2022

Author Contributions:

Conceptualization: Yi-Ying Chen, Sebastiaan Luysaert
Data curation: Chao-Tzuen Cheng, Jing-Shan Hong
Formal analysis: Yi-Ying Chen, Wei Huang
Funding acquisition: Yi-Ying Chen
Investigation: Yi-Ying Chen, Wei Huang, Chao-Tzuen Cheng, Jing-Shan Hong, Fang-Li Yeh
Methodology: Yi-Ying Chen
Supervision: Yi-Ying Chen
Validation: Yi-Ying Chen
Visualization: Wei Huang
Writing – original draft: Yi-Ying Chen
Writing – review & editing: Yi-Ying Chen, Sebastiaan Luysaert

Simulation of the Impact of Environmental Disturbances on Forest Biomass in Taiwan

Yi-Ying Chen¹ , Wei Huang¹ , Chao-Tzuen Cheng² , Jing-Shan Hong³, Fang-Li Yeh^{1,4}, and Sebastiaan Luysaert⁵ 

¹Research Center for Environmental Changes, Academia Sinica, Taipei, Taiwan, ²National Science and Technology, Center for Disaster Reduction, Taipei, Taiwan, ³Central Weather Bureau, Taipei, Taiwan, ⁴Now at Manysplendid Infotech, Taipei, Taiwan, ⁵Department of Ecology, VU, Amsterdam, The Netherlands

Abstract This study seeks to understand the impact on the forest biomass of different kinds of environmental disturbance, including high winds from typhoons, land-use/land-cover changes (LULCC), and CO₂ fertilization. A series of factorial experiments addressing the impact of different types of environmental disturbance on the forest biomass in Taiwan was conducted using the advanced ORCHIDEE-CAN land surface model with a recently developed wind-throw module. The climatic forcing driving the ORCHIDEE-CAN land surface model was first simulated by an atmospheric general circulation model, then dynamically downscaled to a more satisfactory spatial and temporal resolution. The initial and boundary conditions applied in the numerical simulations were based on the long-term CO₂ concentration and LULCC reconstruction, respectively. The model simulation showed an increase in the aboveground wood volume from 209 m³ ha⁻¹ in 1979 to 229 m³ ha⁻¹ in 2017, and the dynamics were consistent with those recorded in the national forest inventory. The annual average carbon sequestration rate over the past 39 years was 0.5 m³ ha⁻¹ yr⁻¹ for a forested area of 2.4 M ha. The most surprising finding was the contribution of the wind disturbance to wood loss, which was at almost the same level as the annual carbon sequestration rate. The LULCC experiment showed a trade-off between afforestation and deforestation in forest biomass accumulation in Taiwan from 1979 to 2017. The CO₂ fertilization effect contributed to an enhancement of forest biomass stock of around 39%, while the CO₂ concentration increased from 296 to 406 ppm over 39 years.

Plain Language Summary Forest biomass is one of the main carbon pools found in terrestrial ecosystems. Its storage capacity is, however, vulnerable to climate change and anthropogenic and natural disturbances. In this study, simulation experiments were carried out to understand the impact of tropical cyclones, land use and land cover change, as well as increasing atmospheric CO₂ concentrations on the forest biomass in Taiwan. The simulation experiments were made possible thanks to century-long country-specific land cover and climate reconstructions, and recent developments of the ORCHIDEE model by the addition of a module capable of simulating the effects of windstorms on forest biomass. Studies show that wind disturbance has a big impact on carbon sequestration rates. In the absence of wind disturbance, the annual sequestration rate would be double that of the present-day rate. In other words, not considering wind disturbances could lead to a significant overestimation of the forest biomass in regions prone to frequent tropical cyclones, some of which can reach typhoon strength.

1. Introduction

One-third of the world's tropical cyclones originate over the Western Pacific Ocean, and almost 90% of these make landfall somewhere in the area (Landsea, 2000). Taiwan is an island situated in East Asia near the coast of mainland China and along the track of tropical cyclones originating in the Western Pacific. Its geolocation makes it a popular area for studies assessing the impact of tropical cyclones on terrestrial ecosystems (Lin et al., 2020). According to historical data reported by Taiwan's Central Weather Bureau (CWB), over the past hundred years the island has been struck by around 3–4 typhoons per year (CWB, n.d.). The strong winds and heavy rainfall brought by typhoons can be very destructive. For example, Typhoon Morakot resulted in an estimated loss to forestry and agriculture of more than 16 billion New Taiwan Dollars (TWD; Yang et al., 2014).

The interaction between the background climate, environmental disturbances, and the forest ecosystem itself, is subtle and complex, and disturbances can trigger multiple succession-disturbance processes (Cannon et al., 2019).

Furthermore, the impact of environmental disturbances in the forest can be worsened by the synergetic effects of natural and anthropogenic forcings within the social-ecological-technological system (Lugo, 2020). For example, frequent land-use/land-cover changes (LULCC), that is, when forested is replaced by other land cover types, can lead to forest degradation, resulting in increased CO₂ emissions from the carbon pool (from harvested wood and organic soils). Past studies have concluded that, following the burning of fossil fuels, emissions due to historical LULCC are the primary sources of an elevation of CO₂ in the atmosphere (Houghton et al., 2012; Li et al., 2017; Pongratz et al., 2009). Increases in atmospheric CO₂ concentrations have been linked to ocean warming (Wang et al., 2014), which in turn affects the frequency and intensity of tropical cyclones (Mei & Xie, 2016). However, it should be noted that forests can also benefit from increased CO₂ concentrations in the atmosphere, by enhancement of their growth rate through photosynthesis. This is known as the CO₂ fertilization effect (Donohue et al., 2013; Farquhar, 1997; Zhu et al., 2016).

The effects of LULCC and CO₂ fertilization are thus included in most dynamic vegetation models (Bayer et al., 2017; Kato et al., 2013; Yue et al., 2018). However, most existing land surface models do not consider tree mortality due to strong wind disturbances. Rather, this type of disturbance is simplified with the invariant background mortality (Smith et al., 2001; Thurner et al., 2017). This simplification has hampered efforts to study the impact of wind disturbance on the forest ecosystem using a modeling approach. Fortunately, the physical process of wind disturbance has been recently implemented in the dynamic vegetation model, ORCHIDEE r4262, allowing for the modeling of abrupt changes in tree mortality in forest stands (Chen et al., 2018). This recent development provides an opportunity to study the impact of wind disturbance on forest biomass, especially in typhoon-prone areas such as Taiwan.

Thus, this study aims to quantify the impact of different types of environmental disturbance, including tropical cyclones, LULCC, and CO₂ fertilization, on the forest biomass in Taiwan by evaluating changes in the aboveground wood volume (AGW) in factorial simulation experiments.

2. Materials and Methods

2.1. Forest Inventory and Environmental Forcing

2.1.1. Forest Inventory

Since 1954, the Forestry Bureau of Taiwan has conducted a forest inventory every 15 to 20 years. At present, the results for the 1954, 1972, 1990, and 2012 inventories are available. Of these inventories, the most recent 2012 inventory not only provides aggregated information but also reports the locations of the sampling plots, enabling a spatially explicit analysis and model evaluation (see Section 2.5).

The sampling plots in the 2012 inventory are almost evenly distributed across the country, including on both private and public forested land. However, the grid spacing used for the plots differs depending upon land ownership, with a 3 km by 3 km grid applied for public forests and a 1.5 km by 1.5 km grid for private forests. Measurements of the number of tree species, the diameter at breast height (DBH), and tree height for all individual living trees with a diameter of more than 6 cm within each 0.05 ha sampling plot are included.

However, a spatially explicit data-model comparison requires identical grid sizes for the data and the models. Because the grid used in the model is determined by the grid of its climate forcing (typically the boundary condition with the coarsest resolution), it is easier to regrid the observations than change the grid in the simulations. The basal area data were taken from the fourth forest inventory, which began in 2008 and was completed in 2012 and included 3,648 plots (Qiu et al., 2015). In this study, the inventoried biomass data were up-scaled to a 5 km by 5 km grid by combining them with high spatial resolution (30 m) canopy height data (Potapov et al., 2021) and in situ basal area data. By using this approach, it is possible to avoid errors introduced by limited samples within the 5 km simulation grid. First, the canopy height data were converted to a coarse resolution by averaging the pixels within a 5 km grid area (Fig. S1a in Supporting Information S1). The up-scaled 5 km canopy height information was then multiplied by the grid averaged basal area (mean value of all observations within the 5 km grid area) to obtain the spatially averaged AGW (Figure S1b in Supporting Information S1). The AGW was estimated by multiplying 0.45, the basal area (BA), and the canopy height (H_c ; $AGW = 0.45 \cdot BA \cdot H_c$) as suggested in the national inventory report.

2.1.2. Land Cover Maps

The model simulations followed the land cover reconstruction process used by Chen et al. (2019). Land cover changes between the years 1904, 1926, 1956, 1980, 1995, 2000, 2005, 2010, and 2015 were reconstructed using various local spatially explicit sources with linear interpolation carried out to show differences in land cover fractions between these years; the land cover was assumed invariant before 1904 and after 2015.

The annual reconstruction distinguished six major land types: forest, grassland, agricultural land, inland water, built-up land, and bare soil. Therefore, to use the reconstruction results as boundary conditions for a land surface model, remapping of six types of land cover as plant functional types (PFTs) was required.

The land cover type, forest, was remapped into three potential PFTs, broad-leaved evergreen tropical, broad-leaved rain-green tropical, and needle leaf evergreen temperate. The vegetation coverage of the different tree species as derived from the forest inventory and local elevations were combined to build the regression model. The fraction of each PFT (Figure S2 in Supporting Information S1) was then estimated by applying the regression model including the altitude (Figure S3 in Supporting Information S1). Data from the fourth forest inventory were fit to this regression model. Built-up and bare soil areas were merged into one plant functional group: bare soil. Grassland and cropland were identified as natural C₃ grass and agricultural C₃ crop type, respectively, in the simulation. The rules applied to remap land cover types as PFTs are summarized in Table S1 in Supporting Information S1.

2.1.3. Climate Forcing

The hourly 5 km by 5 km climate fields, which describe the incoming short-wave and long-wave radiations, near-surface pressure, near-surface specific humidity, surface air temperature, and surface wind speeds, were obtained from the Taiwan Climate Change Projection Information and Adaptation Knowledge Platform project (TCCIP) and Central Weather Bureau (CWB). The climate fields for 1979–2003 were based on the climate projections produced by the Meteorological Research Institute-Atmospheric General Circulation Model version 3.2S (MRI-AGCM3.2S) run at a 20 km horizontal resolution with 60 vertical atmospheric layers up to 0.1 hPa (Mizuta et al., 2017) and observation-based sea surface temperatures from HadISST (Rayner, 2003). Subsequently, the MRI-AGCM3.2S climate projection was downscaled using the Weather Research and Forecasting (WRF) version 3.5.1 software over the region from 150°E–130°E and 15°N–30°N to produce the 5 km by 5 km climate fields.

The climate fields from 2008 to 2017 were extracted from the regional weather forecast system (RFS) operated by the CWB (Chen et al., 2007). An important feature of the RFS is that the rainfall fields are assimilated from real-time radar and in situ measurements which results in more reliable soil moisture conditions (Hung et al., 2014). The long-term annual mean temperature and annual precipitation are shown in Figure S3 in Supporting Information S1. The downscaled hourly windspeed fields at 5 km for eight extreme events (Typhoons Soulik (2013), Nesat (2017), Soudeler (2015), Dujuan (2015), Megi (2016), Matmo (2014), Nepartak (2016), and Meranti (2016)), which occurred from 2013 to 2017, were compared with wind speed observations from the nearest respective CWB meteorological stations. The WRF simulation showed a slight overestimation for winds greater than class 2 on the Beaufort scale. The wind speed realization parameter mean wind ratio (observed wind speed/simulated wind speed, *MWR*) $MWR = 0.7$, was applied to adjust the downscaled daily maximum wind speed in the wind-throw module. For a description of the sensitivity analysis of the introduced model parameter, *MWR*, please see the Supporting Information (Figure S4 in Supporting Information S1).

With the exception of the years 2004 and 2007, for which climate forcing could not be constructed with this method, matching climate fields for the years from 1979 to 2017 were used in the simulation. The gap for the missing years was filled using data from 2008 to 2011. Monthly rainfall and temperature measured by the CWB stations during these two periods show similar patterns, without extreme dry or wet events. Model spin-up and the simulations before 1979 were cycled over the climate fields from 1979 to 1994. This length of period was chosen to include a complete cycle of the south Pacific decadal oscillation (Hsu & Chen, 2011).

2.1.4. CO₂ Concentration

The annual observed atmospheric CO₂ concentrations used in the simulations were based on historical observations (Dlugokencky & Tans, 2020; Keeling et al., 1995). The atmospheric CO₂ concentrations started at 296 ppm in 1900 and had increased to 406 ppm by 2017.

2.2. Model Description

The ORCHIDEE (Organizing Carbon and Hydrology In Dynamic Ecosystems Environment; Bellassen et al., 2010; Krinner et al., 2005) land surface model can be run using any temporal resolution from a minute to a year. However, this apparent flexibility is somewhat restricted because the processes are formalized with given time steps: half-hourly (i.e., photosynthesis and energy budget), daily (i.e., net primary production), and annual (i.e., vegetation dynamics). Hence, meaningful simulations for the energy balance, water balance, and photosynthesis calculations must have a temporal resolution of 15 min to 1 hr. ORCHIDEE builds on the concept of meta-classes to describe the vegetation distribution. By default, 13 meta-classes are distinguished (one for bare soil, eight for forests, two for grasslands, and two for croplands). Each meta-class can be subdivided into an unlimited number of PFTs. For Taiwan, only 6 out of the 28 PFTs defined by ORCHIDEE r4262 are needed (Table S1 in Supporting Information S1).

The biogeochemical and biophysical variables are calculated for each PFT. ORCHIDEE r4262 (Chen et al., 2016; Ryder et al., 2016) is a version of the ORCHIDEE model. In contrast to most land surface models, ORCHIDEE r4262 can simulate dynamic canopy structures, which is essential to simulating the likelihood of wind-throw damage (Chen et al., 2018). Changes in canopy structure resulting from wind-throw are accounted for when calculating the carbon, water, and energy exchange between the land surface and the lower atmosphere. The biomass of the different pools, leaf area index, crown volume, crown density, stem diameter, stem height, and stand density are simulated as accumulated growth for input into the ORCHIDEE r4262 wind-throw module. The critical wind speed is calculated based on the first principles applied in the ForestGALES computer-based support tool (Gardiner et al., 2000) and storm damage is calculated based on the difference between the actual and critical wind speeds, as developed and tested by Anyomi et al. (2017).

At the start of the simulation, each PFT contains a user-defined number of diameter classes. This number is held constant, whereas the boundaries of the classes are adjusted throughout the simulation to accommodate temporal evolution in the structure of the stand. Thus, different forest structures can be simulated using flexible class boundaries with a fixed number of diameter classes. In the simulation, an even-aged forest, for example, is represented as having a small range of diameters between the smallest and largest trees. All trees thus belong to the same stratum.

On the other hand, an uneven-aged forest is simulated by applying an extensive range between the diameter classes. Different diameter classes, therefore, represent different strata. Each diameter class in the model contains a single tree which is replicated to produce realistic stand densities. Following this, tree growth, canopy dimensions, and stand density are updated. Individual tree mortality throughout the simulation causes the stand density to decrease. In ORCHIDEE r4262, individual tree mortality is caused by self-thinning and forest management. In the absence of these processes, a constant rate of environmental background mortality is applied to account for mortality through fires, pests, and wind-throw. However, mortality from wind-throw can now be explicitly accounted for by applying the newly developed wind-throw and storm damage module r4262.

Furthermore, age classes are used to simulate regrowth of the forest after a change in land cover or forest management event. Following a change in the land cover, the biomass and soil carbon pool (but not soil water columns) are either merged or split to represent the various outcomes of the change. This dynamic approach to modeling the structure of the stand and landscape is exploited in other parts of the model, that is, for precipitation interception, transpiration, energy budget calculations, the radiation scheme, absorption of light for photosynthesis, and, for r4262, tree mortality from wind storms. The ORCHIDEE r4262 model was selected as the research tool to conduct all experiments, as detailed in the next section.

2.3. Experimental Design

A series of factorial simulation experiments, EXP.T1, EXP.T2, and EXP.T3, as well as a spin-up experiment (EXP.T0), was designed to quantify changes in forest biomass in Taiwan that occurred in response to historical environmental changes and disturbances:

EXP.T0: this simulation was driven by the relatively cold climatic conditions of 1979, with the land cover state in 1904 assigned as an initial condition to determine the quasi-equilibrium state of the soil carbon pool. The effect of tropical cyclones was also considered by running the model with the wind-throw module over the simulation period. This simulation was designed to run for 300 cyclic years and applied as the initial condition for EXP.T1.

EXP.T1: was a so-called transient simulation designed to account for changes in the soil carbon stock associated with dynamic land cover changes. This simulation started in 1904 running until 1978. The climate fields from 1979 to 1994 are cycled within this 75-year period. This specific 15-year period was chosen because it covers an entire cycle of the south Pacific decadal oscillation, which affects the weather in Taiwan (Hsu & Chen, 2011). Dynamic land cover maps of Taiwan from 1904 to 1978 were used during the simulation period as well as the observed atmospheric CO₂ concentrations. The simulation result was then used as the initial condition for EXP.T2.

EXP.T2 (Control): the aim was to best reproduce the present-day biomass of Taiwan's forest by accounting for land cover changes and natural disturbances such as wind-throw and drought. For this simulation, the historical land cover maps, atmospheric CO₂ concentrations, and matching climate fields were used to drive the model during the period from 1979 to 2017.

EXP.T3: was comprised of three configurations making up the actual attribution experiment. EXP.T3A differed from the control experiment in that the atmospheric CO₂ concentrations were fixed at the 1979 level. EXP.T3B differed from the control simulation in that the land cover was fixed at the 1979 level. EXP.T3C differed from the control experiment in that it did not account for damage from wind-throw. The same climate fields were applied in all three EXP.T3 configurations for the period from 1979 to 2017.

A comparison of EXP.T2 (control run) and EXP.T3 was made revealing the effect of CO₂ fertilization (EXP.T3A), land cover change (EXP.T3B), and wind-throw (EXP.T3C) on the Taiwan forest biomass in the second half of the twentieth century. A simplified factorial set-up was used, which implies that the interaction between the factors (CO₂ fertilization, land cover changes, and wind-throw) cannot be quantified.

2.4. Model Sensitivity

The sensitivity of the wind-throw model was tested by introducing an additional parameter, the mean wind ratio (*MWR*), for correction of the magnitude of the daily maximum wind speed calculation. Eight extreme events including Typhoons Soulik (2013), Nesat (2017), Soudeler (2015), Dujan (2015), Megi (2016), Matmo (2014), Nepartak (2016), and Meranti (2016) during the period from 2013 to 2017 were analyzed. The median *MWR* obtained from the selected extreme events ranged from 0.4 to 1.0. A detailed analysis of the *MWR* calculation can be found in the supplementary data (Figure S4 in Supporting Information S1).

Sensitivity experiments were conducted with different daily maximum wind speed adjustments. The *MWR* was represented by three ranks within the wind-throw module, 0.4, 0.7, and 1.0, with cyclic climatic forcing (1979–1994) before 1979 and historical climatic forcing after 1980, and the land type and CO₂ values were obtained from reconstructed annual land cover maps and global averaged annual mean atmospheric CO₂ concentration. All experiments were restarted from the spin-up experiment (EXP.T0) and simulated across 104 years (1904–2017). Simulated AGWs from all sensitivity experiments are shown in Figure S5 in Supporting Information S1.

2.5. Model Evaluation

Prior to running a simulation experiment, it needs to be established whether the model can reproduce the observational records of critical variables as well as the changes therein. Previous evaluation studies using ORCHIDEE r2290 and r2566 focused on Europe (see Section 4.1, Chen et al., 2016; Luyssaert et al., 2018; Naudts et al., 2015;

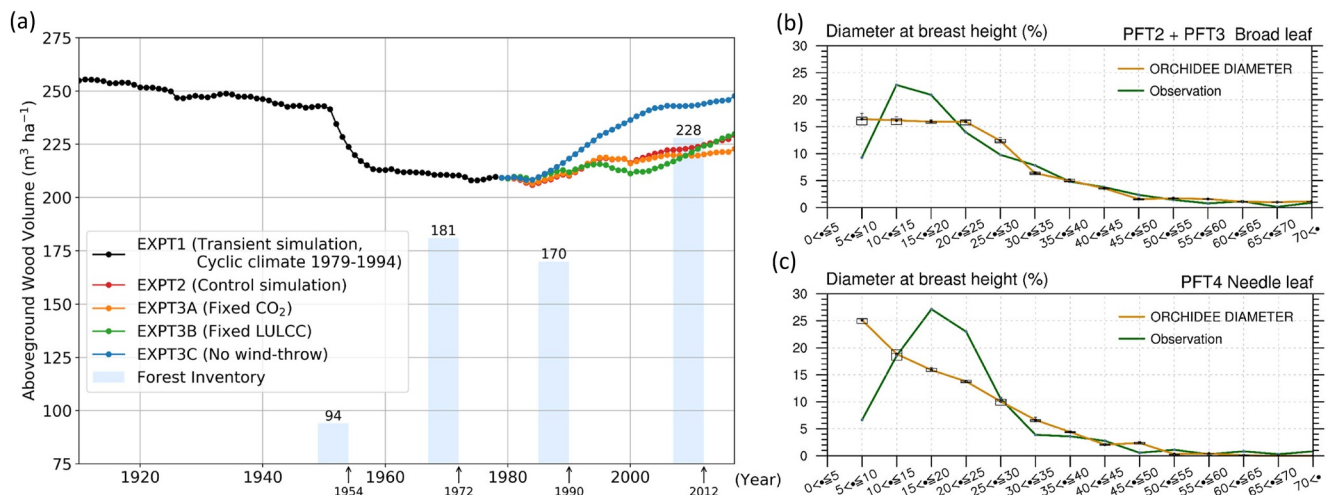


Figure 1. (a) The dynamics of model-simulated forest AGW from the control simulation and forest inventory. Comparison of the observed and model simulated DBH distribution for (b) broad-leaved species (c) and needle leaf species.

Naudts et al., 2016; Ryder et al., 2016) but in this study, the modeling is applied to Taiwan data. It is necessary, therefore, to evaluate whether the model (EXPT2) can reproduce the wood volume and probability density function of the DBH, as well as the number of individuals per unit of ground area as reported in the fourth National Forest Inventory.

3. Results

3.1. Model Evaluation

Between 1979 and 2017, the simulated AGW increased by $20 \text{ m}^3 \text{ha}^{-1}$ from $209 \text{ m}^3 \text{ha}^{-1}$ to $229 \text{ m}^3 \text{ha}^{-1}$. In 2012, the simulated AGW reached $225 \text{ m}^3 \text{ha}^{-1}$ compared to the observed $228 \pm 5 \text{ m}^3 \text{ha}^{-1}$ as reported in the fourth National Forest Inventory (Figure 1a).

A comparison of the simulated and observed DBH distributions of broad-leaved and needle leaf tree species (Figures 1b and 1c, respectively) shows that the model tends to overestimate the number of individual trees with a DBH below 10 cm and underestimate the number of trees for needle leaf species when the DBH ranges from 15 to 25 cm. Consequently, there is a 2 cm difference between the simulated mean DBH and observed mean DBH for the needle leaf tree species, that is, 19 cm in the simulations compared to 21 cm in the observations. The simulated mean DBH for broad-leaved trees is 22 cm, which is quite close to the DBH of 21 cm reported in the fourth National Forest Inventory report.

The spatial distribution of the simulated AGW, as presented in Figure 2a is positively correlated to the up-scaled AGW from the fourth National Forest Inventory (Figure 2a). Both the observed and simulated high wood volume results approach $600 \text{ m}^3 \text{ha}^{-1}$ in the Central Mountain Range. The model calculated 5 km AGW shows a slightly over-estimation (slope = 0.94) with an RMSE of $110 \text{ m}^3 \text{ha}^{-1}$ (see Figure S6 in Supporting Information S1). The large RMSE in Figure S6 in Supporting Information S1 reflects the curvilinear relationship between the model simulation results and in situ observation. The model tends to overestimate the AGW at values from $100 \text{ m}^3 \text{ha}^{-1}$ to $500 \text{ m}^3 \text{ha}^{-1}$ but underestimates AGW at values exceeding $500 \text{ m}^3 \text{ha}^{-1}$.

Three long-term flux observation sites, two secondary broad-leaved forest sites (Lien-Hua-Chi (LHC) and Da-Nong-Da-Fu (DNDF)), and a needle leaf site (Chi-Lan-Mountain (CLM)) were selected for the data-model comparison. Likewise, the AGW of the DNDF afforestation site at Hualien is $100 \text{ m}^3 \text{ha}^{-1}$ (the stand age is nearly 20 years), whereas the simulated AGW is $101 \text{ m}^3 \text{ha}^{-1}$, as indicated by the closed and open red circles in Figures 2 and 2b, respectively. The AGW of the LHC secondary forest site located in central Taiwan is $282 \text{ m}^3 \text{ha}^{-1}$ (the stand age is about 70 years), and the simulated AGW is $166 \text{ m}^3 \text{ha}^{-1}$, as indicated by the closed and open red circles in both Figures 2b and 2c, respectively. The difference is greater for the needle leaf site. The AGW of the

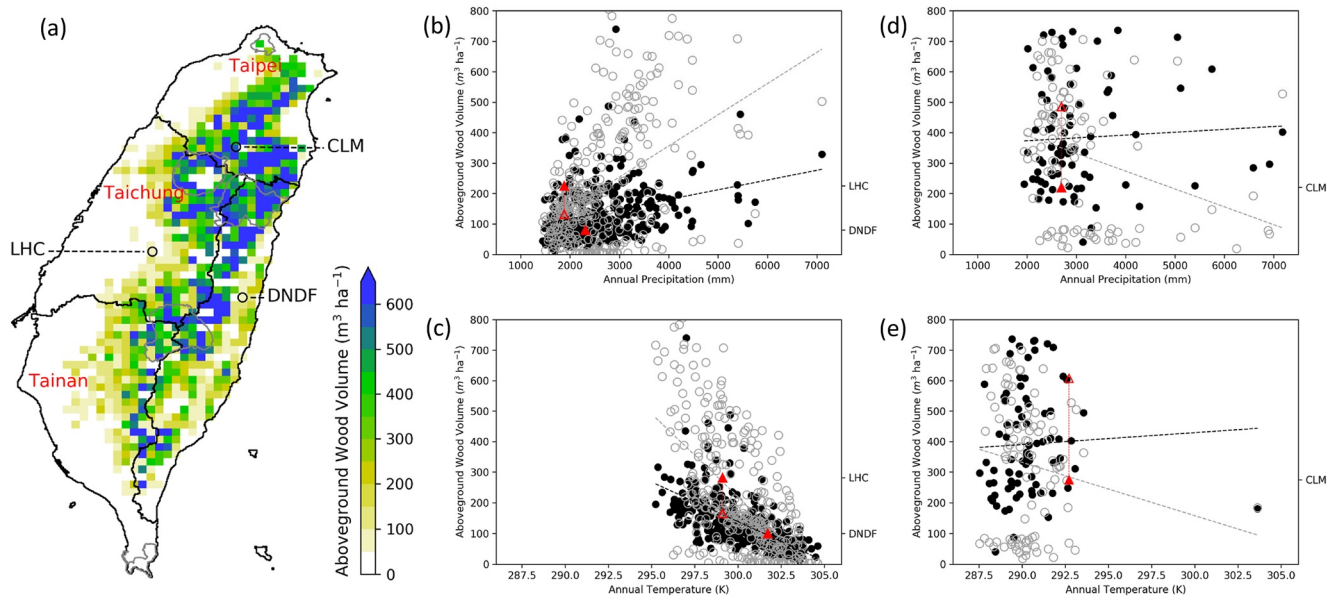


Figure 2. Comparison of model-simulated forest AGW (a) and inventory data. The black and open gray circles indicate the model simulation and inventory data, respectively. One afforestation site, Da-Nong-Da-Fu (DNDF), is in Hualien. Two secondary forest sites are in Lian-Hua-Chih and Ci-Lan-Mountain (LHC and CLM), which were marked with red and open triangles. The subplots show the relationships between precipitation and temperature. Parts (b) and (c) show the data for broad-leaved forests and (d) and (e) for needle leaf forests. The forest biomass in broadleaved forests shows a positive relationship with annual precipitation (see b) and a negative association with annual mean temperature (see c). On the other hand, the forest biomass of needle leaf forests shows a weak correlation with annual precipitation and annual mean temperature (see d and e). The solid black lines in (a) show the borders of the four water resource sectors in Taiwan, and the solid gray lines indicate the boundaries of the five national parks.

CLM site is $275 \text{ m}^3 \text{ ha}^{-1}$, as indicated by the closed red circles (stand age is about 60 years); however, the simulated AGW is $605 \text{ m}^3 \text{ ha}^{-1}$, as indicated by the open red circles in both Figures 2d and 2e.

The observed and simulated biomass of broad-leaved forests show a weakly positive relationship with the precipitation gradient ($\rho = 0.2$, $p < 0.01$ for the observations; $\rho = 0.5$, $p < 0.01$ for the simulation results; Figures 2b and 2a) negative relationship with the temperature gradient ($\rho = -0.5$, $p < 0.01$ for the observations; $\rho = -0.6$, $p < 0.01$ for the simulation results; Figure 2c). However, the observed and simulated biomass for needle leaf forests show no significant correlation with precipitation gradients ($\rho = 0.1$, $p = 0.50$ for the observations; $\rho = -0.2$, $p = 0.12$ for the simulation results; Figure 2d) or temperature ($\rho = -0.1$, $p = 0.99$ for the observations; $\rho = -0.2$, $p = 0.05$ for the simulation results; Figure 2e). These results demonstrate the capability of the model to reproduce the observed relationships between biomass, temperature, and precipitation for forests in Taiwan.

3.2. Impact of Environmental Disturbances on the AGW

The control simulation (EXP.T2) suggests an increase in AGW of $20 \text{ m}^3 \text{ ha}^{-1}$ between 1979 and 2017 due to the combined effects of forest growth, land cover change, CO_2 fertilization, and associated climate change as well as wind-throw (Figure 3a). The factorial simulation experiment shows the impact of CO_2 fertilization, with the contribution of related climate change (EXP.T3A) being $13.6 \text{ m}^3 \text{ ha}^{-1}$. The effect of these environmental changes on forests shows a homogeneous spatial pattern for all forests in Taiwan (Figure 3b).

The LULCC, CO_2 fertilization, and the associated climate change (EXP.T3B) contributed $21 \text{ m}^3 \text{ ha}^{-1}$ between 1979 and 2017. In other words, the afforestation and deforestation LULCC offset each other in terms of forest biomass resulting in a similar net change of AGW ($21 \text{ m}^3 \text{ ha}^{-1}$ vs. $20 \text{ m}^3 \text{ ha}^{-1}$) compared to the control simulation (EXP.T2). The spatial pattern showed an increase of forest biomass in lowland areas and a decrease of forest biomass in the mountainous area due to agricultural expansion and local deforestation (Figure 3c).

The results of the factorial simulation experiment without wind-throw (EXP.T3C) suggest that there would be an accumulation of $38 \text{ m}^3 \text{ ha}^{-1}$ of wood in the absence of tropical cyclones due to the combined effects of forest growth on LULCC, and CO_2 fertilization and the associated climate change. Between 1979 and 2001 tropical

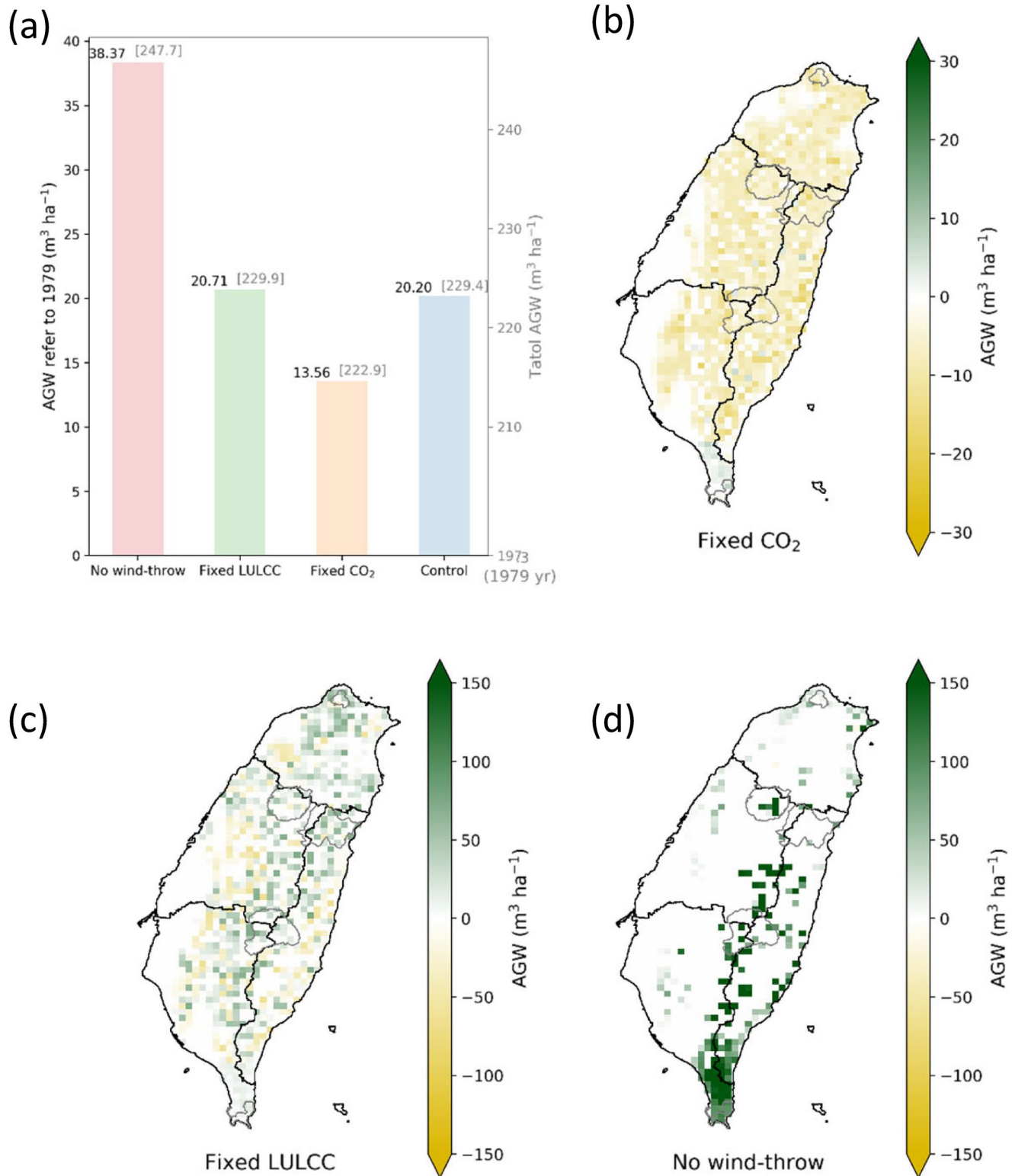


Figure 3. (a) The impact on AGW in the model simulation for different scenarios. The control simulation includes CO_2 fertilization and the associated climate change, land use and land cover changes, as well as wind-throw. (b) Fixed CO_2 (fixed at an atmospheric CO_2 concentration of 1979); (c) fixed LULCC (fixed land cover state in 1979); (d) No wind-throw. The difference in AGW was calculated by comparing the results from the control simulation with different scenarios.

Table 1
Aboveground Wood Volume and Biomass Estimation From in Situ Forest Inventory

Stand age	Vegetation type	Aboveground wood volume (m ³ ha ⁻¹)	Reference
20-year/27-year	Needle leaf Sp.	310/338	Lin et al. (2003)
Secondary forest	Broad-leaved Sp.	186	Lee and Feng (2008)
46-year/26-year	Broad-leaved Sp.	504/216	Lin et al. (2008)
34-year	Needle leaf Sp.	356	Lin and Lin (2008)
50-year	Needle leaf Sp.	>400	Chiu et al. (2011)
10-year (afforestation)	Broad-leaved Sp.	~110	Cheng et al. (2016)

cyclones led to several decreases in AGW. After 2001, however, the impact of individual tropical cyclones on AGW was no longer apparent (Figure 1a). In the simulations, most storm damages occurred in the Central Mountain Range, the southern part of Taiwan, and the coastal areas. In contrast, the simulations showed a slight wood loss in the western part of Taiwan (Figure 3d).

4. Discussion

4.1. Model Evaluation

The model predictions were obtained for the gross primary production (GPP), albedo, transpiration, and surface energy fluxes, all of which have been evaluated in previous studies for Europe (Chen et al., 2016; Naudts et al., 2015, 2016; Otto et al., 2014), without revealing significant differences with the model. For Taiwan, however, the interplay between the current model parameters describing the leaf, root, and sapwood longevity, self-thinning relationship, and diameter-height relationship tended to produce an overestimation of the lower range of AGW. The underestimation of the high range of AGWs was possibly due to the temporal scaling parameter *MWR* used for the wind speed, which resulted in the curvilinear relationship between the model simulation and the in situ observations (Figure S6 in Supporting Information S1). The simulated critical wind speed for stem-breakage of large trees is less than for small trees. Big trees are thus more likely to be removed, resulting in a decrease of AGW. The type of wind damage (such as litterfall as reported by Lin et al. (2017)) is not considered in the wind-throw module, which could also have contributed to this mismatch.

Subsequent model evaluation was made by comparing the results between the observations and the simulated values obtained throughout the study area, that is, Taiwan. Observations of Taiwan's forests have shown an accumulation of AGWs between 110 and 504 m³ ha⁻¹ across different tree species and stand ages (Table 1). The simulation gave an assembled value for the AGW between the third (1990) and fourth (2012) national inventory of 21 ± 4 m³ ha⁻¹ in about 23 years.

The probability density function for the diameter at breast height matches the observations for broad-leaved species (χ test, *p*-value <0.05, *n* = 854) but fails to reproduce the observations for needle leaf species (χ test, *p*-value = 0.5, *n* = 456). However, the observed number of large trees (>25 cm in diameter) which comprise 17% of the total biomass, is consistent with the number simulated by the model. Thus, despite underestimating the number of small trees, the model could simulate the total wood volume. The inconsistency in biomass estimation suggests that the parameters used for the simulated stand structure have a reasonable value for the broad-leaved species but need to be refined for the needle leaf species to enhance the match between the simulation results and observations.

The observations, however, suggest an abrupt increase of AGW, of 85 m³ ha⁻¹, between the first (1954) and second forest inventory (1972; Figure S7 in Supporting Information S1). This steep increase could be the result of significant deforestation of young forests or rapid afforestation by fast-growing species. However, the land cover reconstruction shows only a slight decrease (−1.9%, −397 km²) in forest area.

Although the first and the second national forest inventories were both based on airborne remote sensing observations, the aboveground biomass estimates for the first inventory were made with reference to 545 control plots

Table 2
Statistics for Aboveground Wood Volume (AGW) for Different Regions in Taiwan

Region	Elevation	Area of young forests in this region x 10 ² (ha)	Average AGW (m ³ ha ⁻¹) for low biomass forests	Average AGW (m ³ ha ⁻¹) for the other forests	Potential increase (m ³ ha ⁻¹)
Lowlands	<500 m	6,700	59.7	100.2	40.5
Low elevation mountains	500–800 m	3,000	103.2	171.6	68.4
Montane cloud forests	800–2,500 m	10,475	238.4	300.0	61.6

with different tree species. This difference may be the reason for the abrupt change, rather than this change representing a sudden alteration in forest growth. Given the relatively constant size of the forested area, the increase is likely caused by an increase in productivity per unit of land in 87 m³ ha⁻¹ over a 23-year interval. The increased growth rate of AGW would then be about 3.8 m³ ha⁻¹ yr⁻¹, equivalent to four times the actual growth rate. Enhancement of the growth rate in the early stage of plant development has been documented as possibly due to nitrogen fertilization, irrigation, changes in short rotation coppice, or the thinning of subtropical tree species, within the range from 40% to nearly 200% (Chang et al., 2019; Yen & Li, 2019). However, none of these changes have been documented to have occurred on a sufficiently large scale to explain the increase in AGW between 1954 and 1976. Therefore, we consider it more likely that the AGW based on the 1954 inventory was too low. Another possible reason for the large under-estimation could be the lower sample numbers in mountainous areas inaccessible by public transport at that time. In the latest inventory report the biomass is also observed to be higher at higher altitudes. In this study, the model simulations are designed to assume default forest management (un-managed forests), which would result in an underestimation of the biomass for needle leaf forests. The incorporation of detailed forest management map information might improve the model bias demonstrated by the difference between the simulation results and the reported forest inventory results, especially for the needle leaf forests.

4.2. Present-Day Forest Biomass Distribution

The present-day global average AGW forest biomass (volume of growing stock) is 137 m³ ha⁻¹ while for Asia it is 100 m³ ha⁻¹ (FAO, 2020). The observed forest biomass for Taiwan's forests was 228 m³ ha⁻¹ in 2012 with the simulated value for 2012 estimated to be 225 m³ ha⁻¹. Taiwan's AGW is similar to Japan's (170 m³ ha⁻¹), but around 2–3 times the values reported for other nearby places such as China (85 m³ ha⁻¹), Korea (79 m³ ha⁻¹; Tomppo et al., 2010), or the Chinese province of Fujian (87 m³ ha⁻¹; Xu et al., 2019). Assuming that owners continue to manage their forested land as high-stand growth and there are no changes in land cover, the relatively lower biomass forests (lowest 20% of AGW) could reach the average biomass observed in regions with similar climatic background conditions. Forest management could increase the average AGW by about 40.5 m³ ha⁻¹, 68.4 m³ ha⁻¹, and 61.6 m³ ha⁻¹ for lowlands, lower elevation mountains, and montane cloud forests, respectively (Table 2). Here, it is assumed that the biomass in low biomass forests should be the same or even higher than in mature forests.

The spatial distribution of the simulated forest biomass reproduces the observed gradient, with an AGW of over 300 m³ ha⁻¹ in the central mountainous areas and stocks of less than 100 m³ ha⁻¹ dominant in the lowlands (Figure S1 in Supporting Information S1 and Table 2). The high AGW in the central mountains occurs in the so-called “cloud forests” (Gu, 2020; Schulz et al., 2017), where the ecological conditions support abundant vegetation growth in combination with a low disturbance frequency. Several of these cloud forests, for example, Mt. Peitungyen (McEwan et al., 2011) managed by the National Chung Hsing University and Hapen Creek (Lin et al., 2018), are now protected as nature reserves. However, given the specific ecological requirements, that is, cloud forest conditions and low disturbance frequency, the spatial extent of these high-biomass forests in Taiwan is expected to be somewhat limited.

Previous studies have suggested that extreme rainfall events like those triggered by typhoons and seasonal monsoons, as well as the topography, are essential drivers for forest growth in Taiwan's mountainous areas (Chiu et al., 2018; Lin et al., 2011, 2018; McEwan et al., 2011). When a typhoon passes over the mountains, the wind

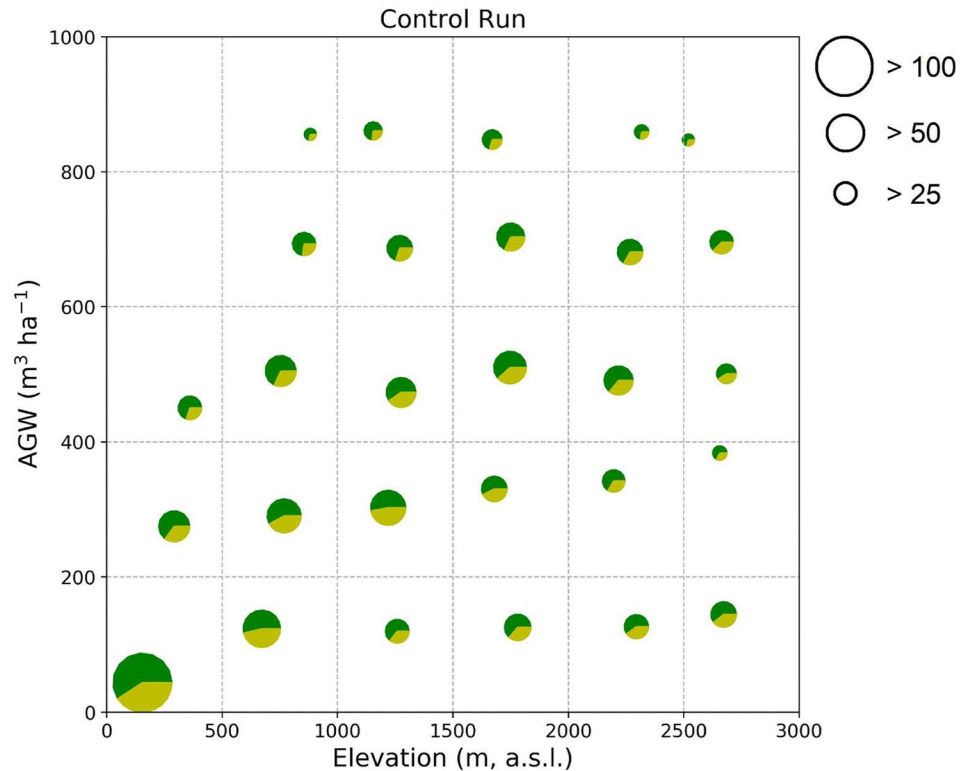


Figure 4. Correlation of calculated aboveground wood volume (AGW) to elevation. The percentage in the pie charts indicates the proportional coverage of needle leaf forest (green) and broad-leaved forest (dark green). The circle size represents the number of simulation grids for each elevation-AGW binning.

speed increases and orographic lifting of the air mass further intensifies rainfall on the mountains' windward side. Given that the typhoons typically travel from east to west, and the geography does not change, it means that the same valleys will be impacted by or protected from high winds. It is expected that this will result in short-statured forests with low biomass, a phenomenon known as dwarfing, in valleys which are exposed to typhoon winds (Lin et al., 2018), while taller forests with high biomass will flourish in the sheltered valleys. In the simulation results, the locations of low biomass in the mountainous areas do coincide with the observed occurrence of extremely high wind speeds (Figure S7 in Supporting Information S1). The results of the control simulation reproduce the large-scale spatial variability in the biomass recorded in the fourth National Forest Inventory.

Another possible reason for the observation that the AGW is higher at higher altitudes is that these areas have mostly been spared from anthropogenic land cover changes. In Taiwan, the vast majority of the population lives near the coast and is reliant on nearby croplands, grasslands, and lowland forests for agriculture. Although the higher mountain ranges have largely been spared changes due to the agricultural expansion, historical land cover reconstruction maps still show a few. The effect of steep terrain on land cover change is reflected in the relationship between the altitude and aboveground biomass (Figure 4). Thus, it can be said that the inaccessibility of the mountain areas has protected the forests from both human exploitation and storm damage. Sheltered conditions are required to develop a high biomass stand in a densely populated region which experiences the passage of approximately four tropical cyclones per year (Wu & Kuo, 1999).

4.3. Historical Changes in Standing Biomass and Vulnerabilities Affecting Biomass Distribution

The model simulation estimated an average AGW of around $250 \text{ m}^3 \text{ ha}^{-1}$ for 1904, when forests covered 65% of the total land area. The AGW gradually decreased to $225 \text{ m}^3 \text{ ha}^{-1}$ together with a decrease in forest cover in the subsequent decades. The lowest level of AGW in the past century (approximately $200 \text{ m}^3 \text{ ha}^{-1}$) occurred around 1980, with land usage for agriculture reaching its maximum extent at that time. The AGW increased from

200 m³ ha⁻¹ to 225 m³ ha⁻¹ along with an increase in forest cover, following a series of nationwide afforestation programs (Forestry Bureau of Taiwan, n.d.) and other measures aimed at protecting the national forests (Forestry Bureau of Taiwan, n.d.). The coupling between AGW per unit of land and the land cover share of forests is striking and suggests that, between 1904 and 1980, high biomass forested areas were converted to agricultural land. The increase in forested area since 1980 is expected to result in a transient decrease in the AGW per unit of area because the newly planted forest must have an AGW well below the national average. This dilution effect is represented in the third National Forest Inventory and is reflected in the simulation, albeit to a lesser degree. Once the newly planted forests reach maturity though, an increase in the average AGW is expected, as seen in both the observations and the simulation results. The factorial simulation experiment suggests that part of this increase is due to CO₂ fertilization and the associated climate change, a response that is well supported by experimental evidence (Albani et al., 2006; Song & Zeng, 2017).

The factorial simulation experiment suggests that over the past 40 years, the frequent occurrence of tropical cyclones has had a more substantial effect on the AGW than the combined effects of land cover change and CO₂ fertilization, or associated climate changes. Thus, even at the national level, a handful of tropical cyclones could offset the impact of decades of afforestation and forest protection programs as well as the effect of enhanced forest growth due to changing environmental conditions. Losses in biomass following the passage of intense tropical cyclones have been well documented (Lin et al., 2003, 2011; Uriarte et al., 2019), although a bias toward studying the most intensive tropical cyclones (class 3 and up; Lin et al., 2020) has resulted in a limited understanding of how forests in storm-prone regions respond to the more frequent passage of lower intensity storms.

However, cyclone intensity is predicted to increase due to global warming, and storm tracks are projected to shift poleward (Mizuta et al., 2017; Tsou et al., 2016; Yin, 2005). Moreover, the translation speed of tropical cyclones has also been slowing down, which could be associated with increased local rainfall and storm-induced damage (Kossin, 2018). More intense storms can be expected to decrease the AGW of Taiwan's forests. On the other hand, if storm tracks move northward it would reduce the frequency of storms making landfall in Taiwan, in which case, an increase in forest biomass could be expected. Similarly, a decrease in the aboveground biomass can be expected in the areas further northward if future storms make landfall.

4.4. Model Limitations

Although nutrient cycling and nutrient limitations do play an important role in tree growth in the (sub)-tropical forest biomes (Houlton et al., 2008), nitrogen (N) and phosphorous (P) cycling are not accounted for in ORCHIDEE r4262. The abundance of dissolved inorganic nitrogen in the river discharge (Chang et al., 2020; Huang et al., 2016) suggests that nitrogen is no longer a factor limiting plant growth over large areas of Taiwan. The primary source of this nitrogen is likely atmospheric deposition from emissions from mainland China, and from local industry and households, estimated to be between 0.8 and 20 kg N ha⁻¹ yr⁻¹ (Zhao et al., 2015). If atmospheric deposition continues to increase in the future, nitrogen saturation in the soil may lead to a decline in forest growth (Aber et al., 2003).

The ideal simulation method would account for both natural and anthropogenic disturbances and the direct and indirect effects of a changing climate (McDowell et al., 2020). In this study, the most critical drivers in determining the growth of Taiwan forests are assumed to be related to the land cover change, unmanaged forests, storm damage, CO₂ fertilization, and climate change. Wildfire could, under certain future climatic conditions, become a substantial disturbing factor in Taiwan, but is not accounted for in this study. Future versions of the ORCHIDEE model are expected to be capable of accounting for fire, drought, floods, windstorms, insect outbreaks, land cover changes, forest management, and the interaction between these disturbances. In this respect, model developments may outrun the empirical evidence, and modelers will soon need datasets that can be used to evaluate the impact of individual disturbances and their interactions.

Data Availability Statement

All model simulation results and field observation data used in this study are publicly available at <https://doi.org/10.5281/zenodo.5717819>.

Acknowledgments

YYC received funding through the Ministry of Science and Technology, R.O.C. (MOST 106-2111-M-001-001-MY3, MOST 108-2111-M-001-001, and MOST 109-2162-M-005). We would like to thank the National Center for High-performance Computing (NCHC) for providing the computational and storage facilities and the Taiwan Forestry Bureau for sharing the fourth national forest inventory data. We thank the two anonymous reviewers and editors for their very helpful observations and suggestions. YYC is grateful for the support received from Dr./Prof. H.-H. Hsu and the mentorship of Dr./Prof. M.-H. Li. YYC would like to thank Mrs. Debbie Nester and Miss Meng-Hsuan Lin for the English proofreading.

References

- Aber, J. D., Goodale, C. L., Ollinger, S. V., Smith, M.-L., Magill, A. H., Martin, M. E., et al. (2003). Is nitrogen deposition altering the nitrogen status of northeastern forests? *BioScience*, 53(4), 375. [https://doi.org/10.1641/0006-3568\(2003\)053\[0375:indatn\]2.0.co;2](https://doi.org/10.1641/0006-3568(2003)053[0375:indatn]2.0.co;2)
- Albani, M., Medvigy, D., Hurtt, G. C., & Moorcroft, P. R. (2006). The contributions of land-use change, CO₂ fertilization, and climate variability to the Eastern US carbon sink. *Global Change Biology*, 12(12), 2370–2390. <https://doi.org/10.1111/j.1365-2486.2006.01254.x>
- Anyomi, K. A., Mitchell, S. J., Perera, A. H., & Ruel, J. C. (2017). Wind-throw dynamics in boreal Ontario: A simulation of the vulnerability of several stand types across a range of wind speeds. *Forests*, 8(7), 1–15. <https://doi.org/10.3390/f8070233>
- Bayer, A. D., Lindeskog, M., Pugh, T. A. M., Anthoni, P. M., Fuchs, R., & Arneeth, A. (2017). Uncertainties in the land-use flux resulting from land-use change reconstructions and gross land transitions. *Earth System Dynamics*, 8(1), 91–111. <https://doi.org/10.5194/esd-8-91-2017>
- Bellassen, V., Maire, G. L., Dhôte, J. F., Ciais, P., & Viovy, N. (2010). Modelling forest management within a global vegetation model—Part 1: Model structure and general behaviour. *Ecological Modelling*, 221(20), 2458–2474. <https://doi.org/10.1016/j.ecolmodel.2010.07.008>
- Cannon, J. B., Henderson, S. K., Bailey, M. H., & Peterson, C. J. (2019). Interactions between wind and fire disturbance in forests: Competing amplifying and buffering effects. *Forest Ecology and Management*, 436(January), 117–128. <https://doi.org/10.1016/j.foreco.2019.01.015>
- Chang, C. T., Shih, Y. T., Lee, L. C., Lee, J. Y., Lee, T. Y., Lin, T. C., & Huang, J. C. (2020). Effects of land cover and atmospheric input on nutrient budget in subtropical mountainous rivers, northeastern Taiwan. *Water (Switzerland)*, 12(10), 2800. <https://doi.org/10.3390/w12102800>
- Chang, H., Yang, H., Zhao, G., Shi, Z., Wang, B., Chen, J., et al. (2019). Effects of nitrogen application and rainfall exclusion on biomass and biomass allocation in saplings from three species of the Fagaceae family in the mid-subtropical region of China. *Acta Ecologica Sinica*, 39(18). <https://doi.org/10.5846/stxb201805291178>
- Chen, C. H., Lin, T. C., & Hwang, J. L. (2007). Variations in the leaf area index and its effect on estimations of primary production in a natural hardwood forest and a Cunninghamia lanceolata plantation at the lienhuachi experimental forest, central Taiwan (in Chinese). *Taiwan Journal of Forest Science*, 22(4), 423–439.
- Chen, Y. Y., Gardiner, B., Pasztor, F., Blennow, K., Ryder, J., Valade, A., et al. (2018). Simulating damage for wind storms in the land surface model ORCHIDEE-CAN (revision 4262). *Geoscientific Model Development*, 11(2), 771–791. <https://doi.org/10.5194/gmd-11-771-2018>
- Chen, Y. Y., Huang, W., Wang, W. H., Juang, J. Y., Hong, J. S., Kato, T., & Luysaert, S. (2019). Reconstructing Taiwan's land cover changes between 1904 and 2015 from historical maps and satellite images. *Scientific Reports*, 9(1), 1–12. <https://doi.org/10.1038/s41598-019-40063-1>
- Chen, Y. Y., Ryder, J., Bastrikov, V., McGrath, M. J., Naudts, K., Otto, J., et al. (2016). Evaluating the performance of land surface model ORCHIDEE-CAN v1.0 on water and energy flux estimation with a single- and multi-layer energy budget scheme. *Geoscientific Model Development*, 9(9), 2951–2972. <https://doi.org/10.5194/gmd-9-2951-2016>
- Cheng, C. H., Huang, Y. H., Menyailo, O. V., & Chen, C. T. (2016). Stand development and aboveground biomass carbon accumulation with cropland afforestation in Taiwan. *Taiwan Journal of Forest Science*, 31(2), 105–118.
- Chiu, C.-M., Chien, C.-T., Nigh, G., & Chung, C.-H. (2018). Influence of climate on tree mortality in Taiwan (Taiwania cryptomerioides) stands in Taiwan. *New Zealand Journal of Forestry Science*, 48(1). <https://doi.org/10.1186/s40490-018-0111-0>
- Chiu, C.-M., Tang, S.-L., Chung, C.-H., & Lin, C.-J. (2011). Effects of thinning strategies on carbon storage and biomass of Taiwan red cypress (*Chamaecyparis formosensis*) plantations. *Quarterly Journal of Chinese Forestry*, 44(3), 385–400.
- CWB. (n.d.). *How many typhoons hit Taiwan per year on average?* Retrieved from July 9, 2021. https://www.cwb.gov.tw/V8/E/K/Encyclopedia/typhoon/typhoon_list02.html#typhoon-15
- Dlugokencky, E., & Tans, P. (2020). *Trends in atmospheric carbon dioxide*. National Oceanic & Atmospheric Administration.
- Donohue, R. J., Roderick, M. L., McVicar, T. R., & Farquhar, G. D. (2013). Impact of CO₂ fertilization on maximum foliage cover across the globe's warm, arid environments. *Geophysical Research Letters*, 40(12), 3031–3035. <https://doi.org/10.1002/grl.50563>
- FAO. (2020). *Global forest resources assessment 2020*. In *Series: Routledge Studies on the Chinese Economy* (Vol. 67). FAO. <https://doi.org/10.4060/ca9825en>
- Farquhar, G. D. (1997). Climate change: Carbon dioxide and vegetation. *Science*, 278(5342), 1411–1413. <https://doi.org/10.1126/science.278.5342.1411>
- Forestry Bureau of Taiwan. (n.d.). *Reforestation and forest products utilization*. Retrieved from February 19, 2021. <https://www.forest.gov.tw/EN/0002671>
- Gardiner, B., Peltola, H., & Kellomäki, S. (2000). Comparison of two models for predicting the critical wind speeds required to damage coniferous trees. *Ecological Modelling*, 129(1), 1–23. [https://doi.org/10.1016/S0304-3800\(00\)00220-9](https://doi.org/10.1016/S0304-3800(00)00220-9)
- Gu, R.-Y. (2020). *The uniqueness of the hydro-climatological cycle in Taiwan's montane cloud-fog forests*. National Taiwan University. <https://doi.org/10.6342/NTU202002018>
- Houghton, R. A., House, J. I., Pongratz, J., Van Der Werf, G. R., Defries, R. S., Hansen, M. C., et al. (2012). Carbon emissions from land use and land-cover change. *Biogeosciences*, 9(12), 5125–5142. <https://doi.org/10.5194/bg-9-5125-2012>
- Houlton, B. Z., Wang, Y.-P., Vitousek, P. M., & Field, C. B. (2008). A unifying framework for dinitrogen fixation in the terrestrial biosphere. *Nature*, 454(7202), 327–330. <https://doi.org/10.1038/nature07028>
- Hsu, H. H., & Chen, Y. L. (2011). Decadal to bi-decadal rainfall variation in the Western Pacific: A footprint of south Pacific decadal variability? *Geophysical Research Letters*, 38(3), 1–6. <https://doi.org/10.1029/2010GL046278>
- Huang, J. C., Lee, T. Y., Lin, T. C., Hein, T., Lee, L. C., Shih, Y. T., et al. (2016). Effects of different N sources on riverine DIN export and retention in a subtropical high-standing island, Taiwan. *Biogeosciences*, 13(6), 1787–1800. <https://doi.org/10.5194/bg-13-1787-2016>
- Hung, Y.-C., Hong, J.-S., Tsay, C.-L., Barlage, M., & Chen, F. (2014). Evaluation of the high resolution land data assimilation system. *Meteorological Society of the Republic of China*, 42(1), 29–48.
- Kato, E., Kinoshita, T., Ito, A., Kawamiya, M., & Yamagata, Y. (2013). Evaluation of spatially explicit emission scenario of land-use change and biomass burning using a process-based biogeochemical model. *Journal of Land Use Science*, 8(1), 104–122. <https://doi.org/10.1080/1747423X.2011.628705>
- Keeling, C. D., Whorf, T. P., Wahlen, M., & van der Plicht, J. (1995). Interannual extremes in the rate of rise of atmospheric carbon dioxide since 1980. *Nature*, 375(6533), 666–670. <https://doi.org/10.1038/375666a0>
- Kossin, J. P. (2018). A global slowdown of tropical-cyclone translation speed. *Nature*, 558(7708), 104–107. <https://doi.org/10.1038/s41586-018-0158-3>
- Krinner, G., Viovy, N., deNoblet-Ducoudré, N., Ogée, J., Polcher, J., Friedlingstein, P., et al. (2005). A dynamic global vegetation model for studies of the coupled atmosphere-biosphere system. *Global Biogeochemical Cycles*, 19(1), 1–33. <https://doi.org/10.1029/2003GB002199>
- Landsea, C. (2000). Climate variability of tropical cyclones: Past, present and future. In R. A. S. Pielke, & R. A. J. Pielke (Eds.), *Storms* (pp. 220–241). Routledge.

- Lee, H. T., & Feng, F. L. (2008). A forest carbon sequestration inventory system: An example of camphor trees in Taiwan. *Taiwan Journal of Forest Science*, 23(SUPPL), 11–22.
- Li, W., Ciais, P., Peng, S., Yue, C., Wang, Y., Thurner, M., et al. (2017). Land-use and land-cover change carbon emissions between 1901 and 2012 constrained by biomass observations. *Biogeosciences*, 14(22), 5053–5067. <https://doi.org/10.5194/bg-14-5053-2017>
- Lin, K.-C., Hamburg, S. P., Wang, L., Duh, C.-T., Huang, C.-M., Chang, C.-T., & Lin, T.-C. (2017). Impacts of increasing typhoons on the structure and function of a subtropical forest: Reflections of a changing climate. *Scientific Reports*, 7(1), 4911. <https://doi.org/10.1038/s41598-017-05288-y>
- Lin, K.-C., Huang, C., & Duh, C. (2008). Study on estimate of carbon storages and sequestration of planted trees in *Zelkova serrata* plantations, Taiwan. *Journal of National Park*, 45–58.
- Lin, K.-C., Wang, C. P., Huang, C. M., Horng, F. W., & Chiu, C. M. (2003). Estimates of biomass and carbon storage in two Taiwan plantations of the Liukuei experimental forest. *Taiwan Journal of Forest Science*, 18(2), 85–94. <https://doi.org/10.7075/TJFS.200306.0085>
- Lin, S., & Lin, C. (2008). Sequestration of Taiwan red pine plantation. *Quarterly Journal of Chinese Forestry*, 41(4), 521–535.
- Lin, S. Y., Shaner, P. J. L., & Lin, T. C. (2018). Characteristics of old-growth and secondary forests in relation to age and typhoon disturbance. *Ecosystems*, 21(8), 1521–1532. <https://doi.org/10.1007/s10021-018-0238-0>
- Lin, T.-C., Hamburg, S. P., Lin, K.-C., Wang, L.-J., Chang, C.-T., Hsia, Y.-J., et al. (2011). Typhoon disturbance and forest dynamics: Lessons from a Northwest Pacific subtropical forest. *Ecosystems*, 14(1), 127–143. <https://doi.org/10.1007/s10021-010-9399-1>
- Lin, T.-C., Hogan, J. A., & Chang, C. T. (2020). Tropical cyclone ecology: A scale-link perspective. *Trends in Ecology & Evolution*, 35(7), 594–604. <https://doi.org/10.1016/j.tree.2020.02.012>
- Lugo, A. E. (2020). Effects of extreme disturbance events: From ecesis to social–ecological–technological systems. *Ecosystems*, 23(8), 1726–1747. <https://doi.org/10.1007/s10021-020-00491-x>
- Luyssaert, S., Marie, G., Valade, A., Chen, Y. Y., Njakou Djomo, S., Ryder, J., et al. (2018). Trade-offs in using European forests to meet climate objectives. *Nature*, 562(7726), 259–262. <https://doi.org/10.1038/s41586-018-0577-1>
- McDowell, N. G., Allen, C. D., Anderson-Teixeira, K., Aukema, B. H., Bond-Lamberty, B., Chini, L., et al. (2020). Pervasive shifts in forest dynamics in a changing world. *Science*, 368(6494). <https://doi.org/10.1126/science.aaz9463>
- McEwan, R. W., Lin, Y. C., Sun, I. F., Hsieh, C. F., Su, S. H., Chang, L. W., et al. (2011). Topographic and biotic regulation of aboveground carbon storage in subtropical broad-leaved forests of Taiwan. *Forest Ecology and Management*, 262(9), 1817–1825. <https://doi.org/10.1016/j.foreco.2011.07.028>
- Mei, W., & Xie, S.-P. (2016). Intensification of landfalling typhoons over the northwest Pacific since the late 1970s. *Nature Geoscience*, 9(10), 753–757. <https://doi.org/10.1038/ngeo2792>
- Mizuta, R., Murata, A., Ishii, M., Shiogama, H., Hibino, K., Mori, N., et al. (2017). Over 5,000 years of ensemble future climate simulations by 60-km global and 20-km regional atmospheric models. *Bulletin of the American Meteorological Society*, 98(7), 1383–1398. <https://doi.org/10.1175/BAMS-D-16-0099.1>
- Naudts, K., Chen, Y. Y., McGrath, M. J., Ryder, J., Valade, A., Otto, J., & Luyssaert, S. (2016). Europe's forest management did not mitigate climate warming. *Science*, 351(6273), 597–600. <https://doi.org/10.1126/science.aad7270>
- Naudts, K., Ryder, J., McGrath, M. J., Otto, J., Chen, Y. Y., Valade, A., et al. (2015). A vertically discretised canopy description for ORCHIDEE (SVN r2290) and the modifications to the energy, water and carbon fluxes. *Geoscientific Model Development*, 8(7), 2035–2065. <https://doi.org/10.5194/gmd-8-2035-2015>
- Otto, J., Berveiller, D., Bréon, F. M., Delpierre, N., Geppert, G., Granier, A., et al. (2014). Forest summer albedo is sensitive to species and thinning: How should we account for this in Earth system models? *Biogeosciences*, 11(8), 2411–2427. <https://doi.org/10.5194/bg-11-2411-2014>
- Pongratz, J., Reick, C. H., Raddatz, T., & Claussen, M. (2009). Effects of anthropogenic land cover change on the carbon cycle of the last millennium. *Global Biogeochemical Cycles*, 23(4), 1. <https://doi.org/10.1029/2009GB003488>
- Potapov, P., Li, X., Hernandez-Serna, A., Tyukavina, A., Hansen, M. C., Kommareddy, A., et al. (2021). Mapping global forest canopy height through integration of GEDI and Landsat data. *Remote Sensing of Environment*, 253, 112165. <https://doi.org/10.1016/j.rse.2020.112165>
- Qiu, L.-W., Huang, Q.-X., Wu, J.-Q., & Xie, X.-T. (2015). Summary of Taiwan forestry investigation report IV (in Chinese). *Taiwan Forestry Journal*, 41(4), 3–13.
- Rayner, N. A. (2003). Global analyses of sea surface temperature, sea ice, and night marine air temperature since the late nineteenth century. *Journal of Geophysical Research*, 108(D14), 4407. <https://doi.org/10.1029/2002JD002670>
- Ryder, J., Polcher, J., Peylin, P., Ottlé, C., Chen, Y. Y., van Gorsel, E., et al. (2016). A multi-layer land surface energy budget model for implicit coupling with global atmospheric simulations. *Geoscientific Model Development*, 9(1), 223–245. <https://doi.org/10.5194/gmd-9-223-2016>
- Schulz, H. M., Li, C. F., Thies, B., Chang, S. C., & Bendix, J. (2017). Mapping the montane cloud forest of Taiwan using 12 year MODIS-derived ground fog frequency data. *PLoS One*, 12(2), 12–15. <https://doi.org/10.1371/journal.pone.0172663>
- Smith, B., Prentice, I. C., & Sykes, M. T. (2001). Representation of vegetation dynamics in the modelling of terrestrial ecosystems: Comparing two contrasting approaches within European climate space. *Global Ecology and Biogeography*, 10(6), 621–637. <https://doi.org/10.1046/j.1466-822X.2001.00256.x>
- Song, X., & Zeng, X. (2017). Evaluating the responses of forest ecosystems to climate change and CO₂ using dynamic global vegetation models. *Ecology and Evolution*, 7(3), 997–1008. <https://doi.org/10.1002/ece3.2735>
- Thurner, M., Beer, C., Ciais, P., Friend, A. D., Ito, A., Kleidon, A., et al. (2017). Evaluation of climate-related carbon turnover processes in global vegetation models for boreal and temperate forests. *Global Change Biology*, 23(8), 3076–3091. <https://doi.org/10.1111/gcb.13660>
- Tomppo, E., Gschwantner, T., Lawrence, M., & McRoberts, R. E. (2010). *National forest inventories: Pathways for common reporting*. <https://doi.org/10.1007/978-90-481-3233-1>
- Tsou, C. H., Huang, P. Y., Tu, C. Y., Chen, C. T., Tzeng, T. P., & Cheng, C. T. (2016). Present simulation and future typhoon activity projection over Western North Pacific and Taiwan/East coast of China in 20-km HiRAM climate model. *Terrestrial, Atmospheric and Oceanic Sciences*, 27(5), 687–703. <https://doi.org/10.3319/TAO.2016.06.13.04>
- Uriarte, M., Thompson, J., & Zimmerman, J. K. (2019). Hurricane María tripled stem breaks and doubled tree mortality relative to other major storms. *Nature Communications*, 10(1), 1–7. <https://doi.org/10.1038/s41467-019-09319-2>
- Wang, S. J., Cao, L., & Li, N. (2014). Responses of the ocean carbon cycle to climate change: Results from an Earth System Climate Model simulation. *Advances in Climate Change Research*, 5(3), 123–130. <https://doi.org/10.1016/j.accre.2014.11.004>
- Wu, C. C., & Kuo, Y. H. (1999). Typhoons affecting Taiwan: Current understanding and future challenges. *Bulletin of the American Meteorological Society*, 80(1), 67–80. [https://doi.org/10.1175/1520-0477\(1999\)080<0067:tacua>2.0.co;2](https://doi.org/10.1175/1520-0477(1999)080<0067:tacua>2.0.co;2)
- Xu, K., Chang, C. T., Tian, Q., Zeng, H., & Xie, J. (2019). Recovery of forest carbon density and carbon storage in a soil-degraded landscape in southeastern China. *European Journal of Forest Research*, 138(3), 397–413. <https://doi.org/10.1007/s10342-019-01177-3>

- Yang, H.-H., Chen, S.-Y. C., Chien, S.-Y., & Li, W.-S. (2014). *Forensic Investigation of typhoon Morakot Disaster: Nansalu and Daniao Village case study (NCDR 102-T28)*.
- Yen, L., & Li, T. (2019). Analysis of thinning effects on different periods after thinning for a Taiwan red cypress (*Chamaecyparis formosensis* Matsum.) plantation. *Quarterly Journal of Forest Research*, *41*(4), 273–284.
- Yin, J. H. (2005). A consistent poleward shift of the storm tracks in simulations of 21st century climate. *Geophysical Research Letters*, *32*(18), 1–n. <https://doi.org/10.1029/2005GL023684>
- Yue, C., Ciais, P., Luyssaert, S., Li, W., McGrath, M. J., Chang, J., & Peng, S. (2018). Representing anthropogenic gross land use change, wood harvest, and forest age dynamics in a global vegetation model ORCHIDEE-MICT v8.4.2. *Geoscientific Model Development*, *11*(1), 409–428. <https://doi.org/10.5194/gmd-11-409-2018>
- Zhao, Y., Zhang, L., Pan, Y., Wang, Y., Paulot, F., & Henze, D. K. (2015). Atmospheric nitrogen deposition to the northwestern Pacific: Seasonal variation and source attribution. *Atmospheric Chemistry and Physics*, *15*(18), 10905–10924. <https://doi.org/10.5194/acp-15-10905-2015>
- Zhu, Z., Piao, S., Myneni, R. B., Huang, M., Zeng, Z., Canadell, J. G., et al. (2016). Greening of the Earth and its drivers. *Nature Climate Change*, *6*(8), 791–795. <https://doi.org/10.1038/nclimate3004>